Metabolic Labeling

International Edition: DOI: 10.1002/anie.201910555
German Edition: DOI: 10.1002/ange.201910555

Metabolic Labeling of Peptidoglycan with NIR-II Dye Enables In Vivo Imaging of Gut Microbiota

Wei Wang[+], Qinglai Yang[+], Yahui Du[+], Xiaobo Zhou, Xiaochen Du, Qiuyue Wu, Liyuan Lin, Yanling Song, Fuyou Li, Chaoyong Yang, and Weihong Tan**

Abstract: *Deepening our understanding of mammalian gut microbiota has been greatly hampered by the lack of a facile, real-time, and in vivo bacterial imaging method. To address this unmet need in microbial visualization, we herein report the development of a second near-infrared (NIR-II)-based method for in vivo imaging of gut bacteria. Using* D*-propargylglycine in gavage and then click reaction with an azide-containing NIR-II dye, gut microbiota of a donor mouse was strongly labeled with NIR-II fluorescence on their peptidoglycan. The bacteria could be readily visualized in recipient mouse gut with high spatial resolution and deep tissue penetration under NIR irradiation. The NIR-II-based metabolic labeling strategy reported herein, provides, to the best of our knowledge, the first protocol for facile in vivo visualization of gut microbiota within deep tissues, and offers an instrumental tool for deciphering the complex biology of these gut "dark matters".*

Our understanding of the diverse physiological and pathological roles of gut microbiota, considered by many as a long-hidden organ, has been making strides in the last two decades. By their inherent involvement in immune and metabolic functions, these intestinal microbes were shown to have broad and profound impacts on nearly every system of their mammalian hosts.[1] However, advancing our knowledge of these biological processes has been seriously obstructed by the technical deficiencies in imaging and tracking intestinal bacteria when real-time and in vivo biogeographical information is required.[2] Needless to say, imaging is uncontested in its ability to allow the study of highly complex and heterogeneous biological systems like the gut microbiota.[3] A competent visualization method can help researchers understand gut microbiota in many aspects, such as microbe–microbe and microbe–host interactions, temporal and spatial organization of bacteria, and more of the bacterial community on the macroscale.[4] The imaging protocol should be not only biocompatible to the oxygen-sensitive gut microbes, but also highly efficient to cover hundreds of different bacterial species, many of which still cannot be cultured or genetically engineered.[5] Furthermore, because the mammalian microbiota is always embedded in thick tissues, the method should have excellent tissue penetration capability to realize in vivo imaging.

Despite these difficulties and challenges, substantial efforts have been made by both chemists and microbiologists in developing imaging techniques for living gut microbiotas. Current strategies can be classified into two categories. One is based on the tracing of genetically engineered bacteria, and the other involves the use of chemical probes tagged onto bacterial surfaces for imaging analysis. Reporter genes used in genetic engineering include fluorescent protein genes,[6] bioluminescence genes (luciferase),[7] and acoustic response genes.[8] The genetically modified bacteria can be tracked longitudinally by different equipment, but each has its own limitations. For example, luciferases and most fluorescent proteins require oxygen for signal production or chromophore maturation, while the hypoxic environment in the intestine dramatically compromises their use in imaging gut bacteria in vivo.[9] Moreover, in vivo bacterial imaging by detecting bioluminescence often had unsatisfactory spatial resolution.[10] Bacteria engineered with acoustic reporter proteins, which could form hollow nanostructures inside bacteria and respond to ultrasound detection, exhibited improved spatial resolution and suitability to anaerobic environment.[11] Notwithstanding these advantages, the use of this method, like other genetic engineering strategies, is limited to genetically modifiable bacteria, which currently

[*] Dr. W. Wang,[+] Dr. Q. Yang,[+] X. Du, Q. Wu, L. Lin, Dr. Y. Song, Prof. C. Yang, Prof. W. Tan
Institute of Molecular Medicine (IMM), Renji Hospital, Shanghai Jiao Tong University School of Medicine, and School of Chemistry and Chemical Engineering, Shanghai Jiao Tong University
Shanghai 200127 (China)
E-mail: cyyang@xmu.edu.cn
tan@chem.ufl.edu

Y. Du,[+] Prof. C. Yang
Collaborative Innovation Center of Chemistry for Energy Materials, The MOE Key Laboratory of Spectrochemical Analysis and Instrumentation, State Key Laboratory of Physical Chemistry of Solid Surfaces, Department of Chemical Biology, College of Chemistry and Chemical Engineering, Xiamen University
Xiamen 361005 (China)

X. Zhou, Prof. F. Li
Department of Chemistry, Fudan University
Shanghai 200433 (China)

Prof. W. Tan
Molecular Science and Biomedicine Laboratory (MBL), State Key Laboratory of Chemo/Biosensing and Chemometrics, College of Chemistry and Chemical Engineering, Hunan University
Changsha 410082 (China)

Dr. Q. Yang[+]
Research Center for Advanced Materials and Biotechnology, Research Institute of Tsinghua University in Shenzhen
Shenzhen 518057 (China)

[+] These authors contributed equally to this work.

Supporting information and the ORCID identification number(s) for the author(s) of this article can be found under: https://doi.org/10.1002/anie.201910555.

account for only a very small proportion of intestinal bacteria. Therefore, it is still impossible to image the whole gut microbiota community using reporter genes. To overcome these limitations, chemical labeling strategies have been developed. One of these methods took advantage of the binding capabilities and specificities of certain antibiotics. Fluorophore-tagged antibiotics stained specific groups of gut bacteria and showed promising imaging results on intestinal tissue sections.[12] However, because of the bactericidal effects of these probes, they could only be used in vitro.[13] Recently, however, metabolic labeling strategies using bioorthogonal chemical probes, including azidosugars and D-amino acid (DAA)-based metabolic probes, have also been employed in imaging gut microbes.[4b,12,14] After a click reaction with alkyne-functionalized fluorophores, this method enabled fluorescent tagging of bacteria and the subsequent imaging of living bacteria in the gut, and the selection of different labeling probes made the imaging of different bacterial groups possible. Nonetheless, the low tissue penetration of regular fluorescence signals excluded their use in in vivo visualization. Recent progress in second NIR window (NIR-II, 1000–1700 nm) fluorescence has demonstrated that NIR-II imaging could achieve deep tissue penetration (up to 20 mm) with superior temporal and spatial resolution,[15] and small NIR-II fluorophores showed great biocompatibilities in imaging.[16] Inspired by such advancements, we herein report an in vivo imaging method for gut microbiota by integrating the strategy of DAA-based metabolic labeling and NIR-II fluorescence imaging.

NIR-II fluorescence has been widely utilized in tumor, brain, stomach, and other deep tissue imaging.[17] However, its use in gut microbial imaging has never been explored, which can be partially attributed to the difficulties in efficient fluorescence tagging of microbiotas. To label the gut microbiota with high coverage, efficiency, and cell compatibility, we employed a DAA-based in vivo metabolic labeling strategy, which we recently developed[18] and integrated it with click reaction (Scheme shown in Figure 1a) using an azide-containing NIR-II dye (IR-FGN, Figure 1b). D-Alanine is a conserved amino acid at the peptidoglycan (PGN) stem peptide of bacteria, and D-amino acid (DAA) with modified side chains, can be tolerated by the enzymes involved in PGN synthesis and used as PGN-specific metabolic labeling probes. Owing to its high specificity and coverage, the D-propargylglycine (DPG, an alkyne-containing DAA, Figure 1b) probe allowed ready labeling of intestinal microbes with the bioorthogonal alkynyl group on their surfaces. Aqueous solutions of DPG (2 × 200 μL, 1 mM) were given to C57BL/6 mice by gavage with an interval of 3 h. Their cecal microbes were then collected, washed and clicked with the IR-FGN, using a protocol that we previously optimized for bacterial samples with minimum microbial cytotoxicity (Supporting Information, Figure S1).[12] The NIR-II dye IR-FGN, the maximum absorption and emission of which were at 745 and 1050 nm, respectively (Figure 1c), was chosen for its high tissue penetration, water solubility, and excellent quantum yield.[19] The resulting microbiota showed strong NIR-II fluorescence signals after the click reaction (Figure 1d), in

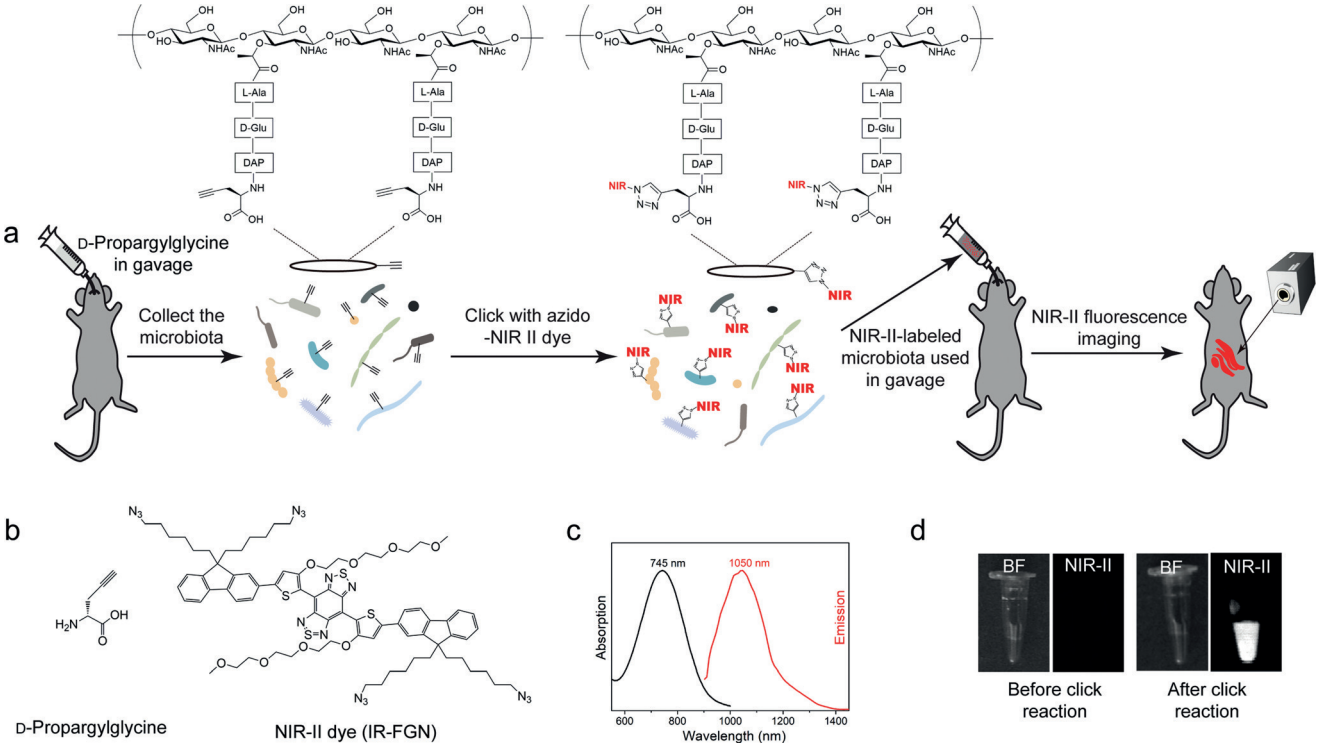

Figure 1. a) Scheme of the NIR-II-based fluorescence imaging of gut microbiota. b) Chemical structures of the metabolic labeling probe D-propargylglycine (DPG) and the NIR-II dye IR-FGN used in this study. c) The normalized absorption and emission spectra of the IR-FGN used in this study. The spectra were measured with 5.0 μL of 10 mM IR-FGN DMSO solution dispersed in 500 μL of water. d) Imaging of DPG-labeled microbiota before and after click reaction with IR-FGN under bright-field (BF) or NIR-II illumination (under 730 nm excitation, signals collected with wavelength > 1100 nm, exposure time: 100 ms).

which the IR-FGN concentration was about 16 μM (Supporting Information, Figure S2). In a control group, L-propargylglycine (LPG), which could not metabolically label bacteria,[20] was used in mouse gavage. In contrast to DPG-labeled microbiota, the LPG-labeled gut microbiota showed very low level of fluorescence after click reaction (Supporting Information, Figure S3), which might be resulted from non-specific binding of the fluorophore to the bacteria. This indicated that the NIR-II signals from DPG-labeled microbiota were from the covalently modified PGN of the bacteria. Compared with other chemical fluorescence-tagging methods for cells, such as the protocol using reactive fluorophores to directly react with amino groups on bacterial surfaces,[21] our metabolic labeling strategy allowed precise labeling of PGN. In an attempt to improve click reaction efficiency, a polyethylene glycol (PEG)-modified NIR-II dye (structure shown in Figure S4 in the Supporting Information), which had the same fluorophore, but with higher aqueous solubility,[19] was used in the click reaction. It was, however, disappointing that the PEG-modified dye somehow showed lower fluorescence intensity compared with the dye without extra PEG modifications (Supporting Information, Figure S5), perhaps because the PEG sterically interfered with the reaction. Therefore, the NIR-II dye without extra PEG was used in the following experiment. Overall, our results established that mouse gut microbiota can be facilely and efficiently labeled with the NIR-II dye IR-FGN by in vivo DAA-based metabolic labeling strategy followed by bioorthogonal click reactions.

Following giving the NIR-II-labeled microbiota to recipient mouse by gavage, a series of in vivo imaging was carried out for visualizing gut microbiota, using a 730 nm laser as the excitation source and an InGaAs CCD as the signal collector. Specific pathogen-free (SPF) BALB/c nude mice were first used as recipients in order to eliminate the reflection of mouse fur. Because of the low autofluorescence and photon scattering in the >1000 nm window of NIR-II fluorescence,[22] the resulting high spatial resolution enabled vivid and clear observation of the biogeography of gut microbes inside mouse intestines through intact abdominal skin. Images were taken at different time points to visualize the longitudinal distributions of the microbiota. Three hours after gavage, the bacteria mostly showed in the duodenum, but by 5 h, the signals were concentrated in different sections of the small intestines. The most dramatic images were observed at 8 h after gavage, where 6–7 segments of the small intestines and possibly cecum could be clearly observed. By 11 h, due to the decay of the PGN labeling, the bacterial fluorescence was decreased and mainly localized in the cecum and colon (Figure 2a). The digestive tract of the mouse, together with some of the other major organs, was then dissected and imaged. Along the small intestine, the fluorescence signals mostly stayed in distal jejunum and ileum, but not in proximal jejunum, probably because of the fast emptying of the latter. Besides the intestines, the signals were also found in liver and spleen (Supporting Information, Figure S6). This could be explained by the degraded bacterial PGN, which had been labeled by the IR-FGN, entering the circulation through the hepatic portal system. Taken together, these data showed that the NIR-II imaging strategy, facilitated by the use of PGN metabolic labeling, allowed clear observation of the biogeography of the gut microbiota in the extensively used SPF mouse model. Because the labeled microbiota was given to the recipient mice by gavage, some of the bacteria might not survive during the process due to the stomach acid and bile acid encountered by the microbes. To determine to which extent the observed fluorescence signals were resulted from living bacteria, recipient mouse was gavaged with NIR-II labeled microbioa that had been killed by ethanol, and imaged. The dead microbiota presented dispersed fluorescence signals in the gut, without any clear outlines of the intestinal track (Supporting Information, Figure S7). The dramatically different fluorescence signals presented by the dead microbiota suggested that the vivid imaging of the transplanted bacteria shown in Figure 2 were mainly from living microbes.

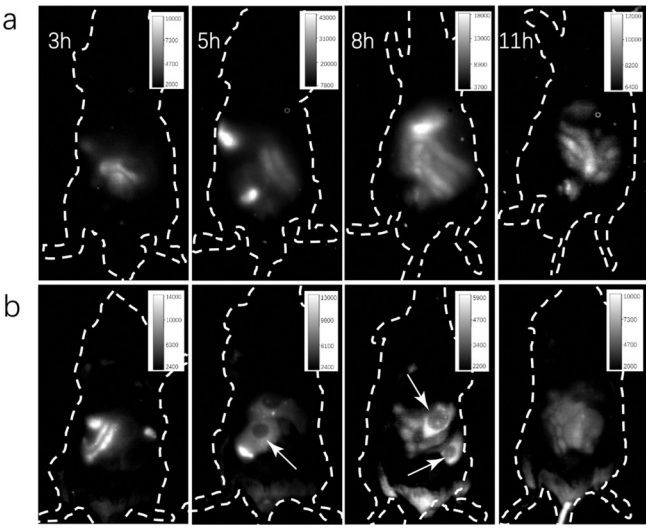

Figure 2. NIR-II-based fluorescence imaging of labeled gut microbiota at different time points following transplantation in SPF (a) and GF mouse (b) (under 730 nm excitation, signals collected with wavelength >1100 nm, exposure time: 100 ms). Representative images from at least three independent experiments were shown.

Besides SPF mouse, germ-free (GF) mouse has been widely employed in microbiota research to validate the causality after being given specific bacteria or microbiota of interest by gavage.[23] Therefore, the ability to track transplanted bacteria in the GF mouse is important to researchers. By administering NIR-II-labeled microbiota in gavage to a group of GF C57BL/6 mice, we were able to visualize the localization of the transplanted bacteria. Mouse abdomen was depilated before imaging to reduce fur reflection. Compared with the SPF mouse, stronger fluorescence in more intestinal areas was observed by 3 h, and during the period of 5–8 h, the microbiota seemed to stay longer in the gut, and even the gas in the small intestines, which was often seen in the gut of GF mice after they were exposed to bacteria, could be clearly observed (Figure 2b, arrows). By 11 h, the bacteria reached the cecum, which was much larger than that of the SPF mouse and could be visualized with unprecedented resolution, together with the pellets stored in the gut (Figure 2b). The labeled gut microbiota showed stronger signals in GF mouse,

when compared to SPF mouse, most likely because of the larger cecal volume and the absence of competition from the original microbiota in SPF animals.

To extend the use of this chemical strategy to a broader scope of microbiology, we went on to test its feasibility in imaging specific bacterial species in the gut. Two commensal and a pathogenic bacteria were NIR-II-labeled in vitro and given to recipient mice by gavage, respectively. A similar labeling strategy was adopted whereby DPG was supplemented to the bacterial culture medium, and IR-FGN was tagged onto the bacterial surface by click chemistry afterwards. As shown in Figure 3, the three bacterial species (two

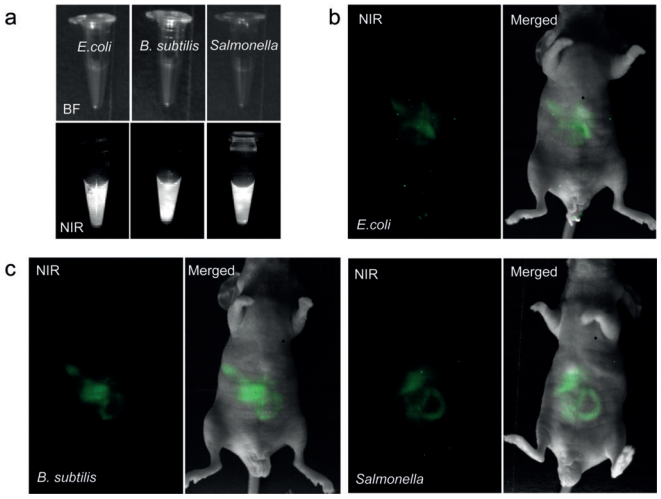

Figure 3. NIR-II-based fluorescence imaging of labeled bacterial species following transplantation in SPF mouse. a) NIR-II imaging showed that three bacterial species, *Escherichia coli*, *Bacillus subtilis*, and *Salmonella enterica serovar* Typhimurium, metabolically labeled by DPG in vitro, all showed strong fluorescence after click with IR-FGN. b–d) In vivo NIR-II imaging of the labeled bacteria 5 h after the gavage of corresponding bacterial species (under 730 nm excitation, signals collected with wavelength >1100 nm, exposure time: 100 ms). Representative images from at least three independent experiments were shown.

Gram-negative and one Gram-positive species) could all be NIR-II-labeled in vitro (LPG labeled control shown in Figure S8 in the Supporting Information) and clearly visualized in vivo after intragastric administration to mice. Currently, the most used method for in vivo bacterial imaging is based on bioluminescence.[10] This requires genetic engineering of the target bacteria and the presence of oxygen to produce signals, both of which meet great challenges in imaging gut bacteria in vivo. In contrast, our imaging strategy is immune to these problems, and the spatial resolution is much higher compared with that of bioluminescence-based imaging in the gut.[7]

Taking advantage of our in vivo microbiota imaging strategy, which enabled facile, real-time assessment of the gut microbial movement, we went on to approach a long-asked question regarding gastrointestinal (GI) motility and its effect on the movement and localization of gut microbiota. Because of its involvement in many diseases, like irritable bowel syndrome, constipation, or small bowel bacterial overgrowth syndrome, the relationship between GI peristalsis and gut microbiota has been extensively studied in neurogastroenterology.[24] Previous investigations of these reciprocal interactions used methods like measuring ink propulsion rates or defecating time by collecting fecal pellet output,[25] which were often invasive or indirect. Here, by using our NIR-II-based imaging method, we were able to directly compare microbiota distributions in different groups of mice treated with loperamide or domperidone, which could either slow down or accelerate GI movement. The drugs were given to mice by gavage 30 min before receiving the labeled microbiotas. As shown in Figure 4, gut microbes showed distinct distribution patterns in the two groups. In the domperidone-treated mouse, the microbiota reached cecum in <8 h after

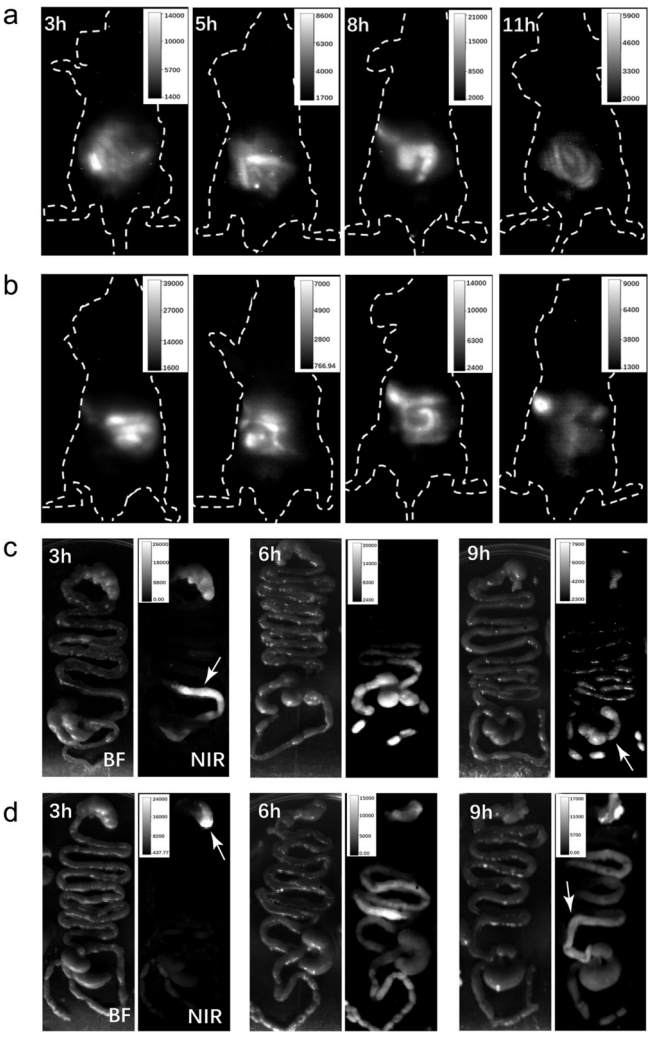

Figure 4. NIR-II fluorescence imaging showed that GI peristalsis dramatically affected the biogeography of gut microbiota. Visualization of the NIR-II-labeled microbiota in the gut of mice treated with domperidone (a) or loperamide (b). Ex vivo NIR-II imaging of the administered microbiotas in the intestines of domperidone- (c) or loperamide-treated (d) mice (under 730 nm excitation, signals collected with wavelength >1100 nm, exposure time: 100 ms). Representative images from at least three independent experiments were shown.

gavage (Figure 4a), while in the loperamide-treated mouse, most signals remained in the small intestines, especially in ileum (Figure 4b). The movement of microbiota caused by GI peristalsis was also captured on video in the domperidone-treated mouse, the fluorescence signals of which could be clearly observed in real time (Supplementary Materials). To examine the affected bacterial biodistributions more closely, in another two groups of mice, the treated animals were sacrificed at each time point, and their digestive tracts were dissected and imaged directly. Microbiota in the domperidone-treated mouse arrived at ileum by 3 h after gavage (arrow, Figure 4c), but most bacteria had not even left the stomach in the loperamide group (arrow, Figure 4d). By 9 h, the bacteria either reached the large intestines or had already been defecated in the domperidone-treated mouse (arrow, Figure 4c), while most microbiota was still in the small intestines in the loperamide group (arrow, Figure 4d). Taken together, these data suggested that the biogeography of gut microbiota could be greatly impacted by GI movements and that the imaging strategy proposed here could assist in studies where GI and microbiota movements were of interest.

In summary, we have established an in vivo imaging method to fulfill the unmet need for gut microbiota visualization by integrating the strategy of DAA-based metabolic labeling and NIR-II fluorescence imaging. DAA-based metabolic labeling enables facile and precise labeling of both microbiotas and individual bacterial species, some of which may not be cultured or genetically engineered. The enhanced imaging depth and high spatial resolution resulted from the NIR-II fluorescence, allows real-time and vivid observation of the bacteria embedded in deep tissues. The applicability of this technique was also demonstrated in the study of GI motility-induced gut microbiota biogeography changes. Further development of this method to allow longer observation window will enable more microbiota analyses such as competition experiment between different bacterial groups for example, which will greatly increase the power of this methodology. We envision that this new imaging strategy will be versatile and instrumental to a variety of microbiology studies and pave a new way for a deeper understanding of gut microbiota.

Acknowledgements

We are grateful to the National Science Foundation of China (21807070, 21735004, 81801749, 21775128, 21705024, and 21521004) and Shenzhen Basic Research funding (JCYJ20170307151634428) for the financial support.

Conflict of interest

The authors declare no conflict of interest.

Keywords: GI peristalsis · gut microbiota · in vivo imaging · microbial biogeography · NIR-II

How to cite: *Angew. Chem. Int. Ed.* **2020**, *59*, 2628–2633
Angew. Chem. **2020**, *132*, 2650–2655

[1] F. Sommer, F. Bäckhed, *Nat. Rev. Microbiol.* **2013**, *11*, 227–238.
[2] G. P. Donaldson, S. M. Lee, S. K. Mazmanian, *Nat. Rev. Microbiol.* **2016**, *14*, 20–32.
[3] a) J. S. Biteen, P. C. Blainey, Z. G. Cardon, M. Chun, G. M. Church, P. C. Dorrestein, S. E. Fraser, J. A. Gilbert, J. K. Jansson, R. Knight, *ACS Nano* **2016**, *10*, 6–37; b) D. Muriel, J. E. T. van Hylckama Vlieg, *Trends Microbiol.* **2015**, *23*, 354–366.
[4] a) K. A. Earle, G. Billings, M. Sigal, J. S. Lichtman, G. C. Hansson, J. E. Elias, M. R. Amieva, K. C. Huang, J. L. Sonnenburg, *Cell Host Microbe* **2015**, *18*, 478–488; b) N. Geva-Zatorsky, D. Alvarez, J. E. Hudak, N. C. Reading, D. Erturk-Hasdemir, S. Dasgupta, U. H. von Andrian, D. L. Kasper, *Nat. Med.* **2015**, *21*, 1091–1100; c) Y. A. Millet, A. David, R. Simon, U. H. von Andrian, B. M. Davis, M. K. Waldor, *PLOS Pathog.* **2014**, *10*, e1004405.
[5] A. W. Walker, S. H. Duncan, P. Louis, H. J. Flint, *Trends Microbiol.* **2014**, *22*, 267–274.
[6] a) B. Lim, M. Zimmermann, N. A. Barry, A. L. Goodman, *Cell* **2017**, *169*, 547–558; b) W. R. Whitaker, E. S. Shepherd, J. L. Sonnenburg, *Cell* **2017**, *169*, 538–546.
[7] a) M. L. Foucault, L. Thomas, S. Goussard, B. R. Branchini, C. Grillot-Courvalin, *Appl. Environ. Microbiol.* **2010**, *76*, 264–274; b) D. Catherine, P. Sabine, D. Véronique, B. Denise, P. Bruno, *Appl. Environ. Microbiol.* **2013**, *79*, 1086–1094.
[8] R. W. Bourdeau, A. Lee-Gosselin, A. Lakshmanan, A. Farhadi, S. R. Kumar, S. P. Nety, M. G. Shapiro, *Nature* **2018**, *553*, 86–90.
[9] J. M. Landete, M. Medina, J. L. Arqués, *World J. Microbiol. Biotechnol.* **2016**, *32*, 119.
[10] M. Barbier, J. Bevere, F. H. Damron, *Methods Mol. Biol.* **2018**, *1790*, 87–97.
[11] G. J. Lu, A. Farhadi, A. Mukherjee, M. G. Shapiro, *Curr. Opin. Chem. Biol.* **2018**, *45*, 57–63.
[12] W. Wang, Y. Zhu, X. Chen, *Biochemistry* **2017**, *56*, 3889–3893.
[13] a) W. Wang, X. Chen, *Sci. China Chem.* **2018**, *61*, 792–796; b) W. Wang, Y. Wang, L. Lin, Y. Song, C. J. Yang, *Anal. Bioanal. Chem.* **2019**, *411*, 4017–4023.
[14] J. E. Hudak, D. Alvarez, A. Skelly, U. H. von Andrian, D. L. Kasper, *Nat. Microbiol.* **2017**, *2*, 17099.
[15] a) K. Welsher, Z. Liu, S. P. Sherlock, J. T. Robinson, Z. Chen, D. Daranciang, H. Dai, *Nat. Nanotechnol.* **2009**, *4*, 773; b) G. Hong, J. C. Lee, J. T. Robinson, U. Raaz, L. Xie, N. F. Huang, J. P. Cooke, H. Dai, *Nat. Med.* **2012**, *18*, 1841.
[16] a) Q. Yang, Z. Hu, S. Zhu, R. Ma, H. Ma, Z. Ma, H. Wan, T. Zhu, Z. Jiang, W. Liu, L. Jiao, H. Sun, Y. Liang, H. Dai, *J. Am. Chem. Soc.* **2018**, *140*, 1715–1724; b) Q. Yang, Z. Ma, H. Wang, B. Zhou, S. Zhu, Y. Zhong, J. Wang, H. Wan, A. Antaris, R. Ma, X. Zhang, J. Yang, X. Zhang, H. Sun, W. Liu, Y. Liang, H. Dai, *Adv. Mater.* **2017**, *29*, 1605497; c) H. Wan, J. Yue, S. Zhu, T. Uno, X. Zhang, Q. Yang, K. Yu, G. Hong, J. Wang, L. Li, Z. Ma, H. Gao, Y. Zhong, J. Su, A. L. Antaris, Y. Xia, J. Luo, Y. Liang, H. Dai, *Nat. Commun.* **2018**, *9*, 1171; d) A. L. Antaris, H. Chen, K. Cheng, Y. Sun, G. Hong, C. Qu, S. Diao, Z. Deng, X. Hu, B. Zhang, X. Zhang, O. K. Yaghi, Z. R. Alamparambil, X. Hong, Z. Cheng, H. Dai, *Nat. Mater.* **2015**, *15*, 235.
[17] a) J. T. Robinson, G. Hong, Y. Liang, B. Zhang, O. K. Yaghi, H. Dai, *J. Am. Chem. Soc.* **2012**, *134*, 10664–10669; b) S. He, J. Song, J. Qu, Z. Cheng, *Chem. Soc. Rev.* **2018**, *47*, 4258–4278; c) Y. Cai, Z. Wei, C. Song, C. Tang, W. Han, X. Dong, *Chem. Soc. Rev.* **2019**, *48*, 22–37.
[18] W. Wang, L. Lin, Y. Du, Y. Song, X. Peng, X. Chen, C. J. Yang, *Nat. Commun.* **2019**, *10*, 1317.
[19] S. Zhu, Q. Yang, A. L. Antaris, J. Yue, Z. Ma, H. Wang, W. Huang, H. Wan, J. Wang, S. Diao, B. Zhang, X. Li, Y. Zhong, K.

Yu, G. Hong, J. Luo, Y. Liang, H. Dai, *Proc. Natl. Acad. Sci. USA* **2017**, *114*, 962 – 967.
[20] E. Kuru, H. V. Hughes, P. J. Brown, E. Hall, S. Tekkam, F. Cava, M. A. de Pedro, Y. V. Brun, M. S. Vannieuwenhze, *Angew. Chem. Int. Ed.* **2012**, *51*, 12519 – 12523; *Angew. Chem.* **2012**, *124*, 12687 – 12691.
[21] a) W. Reinhard, B. Annett, B. Markus, B. Yvonne, H. Thomas, H. Bastian, L. Madeleine, P. Alexander, R. Reinhard, S. Christina, *Appl. Environ. Microbiol.* **2011**, *77*, 1556 – 1562; b) A. Bandyopadhyay, K. A. Mccarthy, M. A. Kelly, J. Gao, *Nat. Commun.* **2015**, *6*, 6561.
[22] S. Diao, G. Hong, A. L. Antaris, J. L. Blackburn, K. Cheng, Z. Cheng, H. Dai, *Nano Res.* **2015**, *8*, 3027 – 3034.
[23] a) P. Luczynski, K. A. McVey Neufeld, C. S. Oriach, G. Clarke, T. G. Dinan, J. F. Cryan, *Int. J. Neuropsychopharmacol.* **2016**, *19*, pyw020; b) M. Grover, P. C. Kashyap, *Neurogastroent. Motil.* **2014**, *26*, 745 – 748; c) R. Martín, L. G. Bermúdez-Humarán, P. Langella, *Front. Microbiol.* **2016**, *7*, 409.
[24] a) D. Neelendu, V. E. Wagner, L. V. Blanton, J. Cheng, L. Fontana, H. Rashidul, A. Tahmeed, J. I. Gordon, *Cell* **2015**, *163*, 95; b) A. Shin, G. A. Preidis, R. Shulman, P. C. Kashyap, *Clin. Gastroenterol. Hepatol.* **2019**, *17*, 256 – 274.
[25] a) T. Murakami, K. Kamada, K. Mizushima, Y. Higashimura, K. Katada, K. Uchiyama, O. Handa, T. Takagi, Y. Naito, Y. Itoh, *Digestion* **2017**, *95*, 55 – 60; b) H. Cao, X. Liu, Y. An, G. Zhou, Y. Liu, M. Xu, W. Dong, S. Wang, F. Yan, K. Jiang, *Sci. Rep.* **2017**, *7*, 10322.

Manuscript received: August 18, 2019
Revised manuscript received: November 9, 2019
Accepted manuscript online: December 2, 2019
Version of record online: January 9, 2020

